NON-COVALENT INTERACTIONS OF β-CHITIN: QUANTUM CHEMICAL CALCULATIONS, HIRSHFELD SURFACE AND FINGERPRINT PLOT ANALYSIS

FERIDE AKMAN

Vocational School of Food, Agriculture and Livestock, Bingol University, 12000 Bingol, Turkey
Institute of Sciences, Bingol University, 12000 Bingol, Turkey
✉ *Corresponding author: F. Akman, chemakman@gmail.com*

Received August 15, 2024

In this investigation, non-covalent interactions in β-chitin were studied using a combination of computational and crystallographic methods. Specifically, non-covalent interactions were assessed through RDG and IRI analysis and compared with Hirshfeld surfaces and fingerprint plots derived from the crystal structure. Theoretical computations of β-chitin were carried out using the DFT approach with the B3LYP/6-31G (d,p), LC-BYLP/6-31G (d,p), and M06-2X/6-31G(d,p) basis sets. In addition, we analyzed the molecular electrostatic potential (MEP) and average local ionization energy (ALIE) surfaces to pinpoint nucleophilic and electrophilic regions. We also examined electron density likelihood at bonding and anti-bonding sites by analyzing Electron Localization Function (ELF) and Localised Orbital Locator (LOL) plots.

Keywords: β-chitin, crystal structure, surface analysis, non-covalent interactions, quantum chemistry, DFT

INTRODUCTION

Natural polymers have been extensively studied for their biotechnological and biomedical potential due to their unique characteristics, such as non-toxicity, degradability, and biological compatibility.[1-4] Natural polymers have the ability to form hydrogen bonds.[5,6] Hydrogen bonding serves as a non-covalent interaction of significance in both chemical and biochemical processes.[7] This characteristic enables the molecules to achieve solubility and establish specific interactions with diverse molecules. Within natural polymer molecules, the proximity of donor and acceptor groups in the chains facilitates the potential for an equilibrium to occur between closed conformations, leading to intramolecular hydrogen bonding and the formation of temporary ring systems.[7,8]

Chitin, also referred to as poly(N-acetyl-D-glucosamine), is the second most prevalent structural polysaccharide in nature, following cellulose. It displays a replenishment rate twice that of cellulose.[9,10] Chitin primarily exists as a fibrillar crystalline material and can be found in three crystalline forms: α-chitin, which consists of alternately antiparallel arranged chains, β-chitin, which features chains arranged in a parallel manner, and γ-chitin, which consists of two chains in one direction with an additional inverted chain. β-Chitin, derived from squid pens, takes a monoclinic form with parallel chains, resulting in weaker intermolecular interactions compared to α-chitin.[11-13] As a result, β-chitin is more susceptible to dissolution in various solvents, making it more reactive and versatile.

Chitin's insolubility in most common organic solvents is due to its strong intra- and inter-molecular hydrogen bonding.[13-16] These exceptional attributes of beta chitin, combined with its robust intramolecular and intermolecular interactions, motivated us to theoretically address this knowledge gap in the literature. For this purpose, surface analysis and non-covalent interactions were investigated using the crystal structure of beta chitin. Hirshfeld surface analysis is a powerful method that allows the observation of intermolecular interactions within a crystal structure. It is known for its unique capability to visually represent and calculate these interactions, producing unique outcomes for each crystal structure analyzed. In quantum studies investigating covalent and non-covalent interactions, it was found that the meta-hybrid

GGA functional was most accurately defined with the M06-2X level.[17] For this reason, we used the M06-2X method in our calculations. The novelty of this work lies in understanding the non-covalent interactions of β-chitin through both quantum chemical calculations and Hirshfeld surface analyses.

EXPERIMENTAL

Computational calculations

The crystal structure of β-chitin (CCDC code: 1425611) was obtained from the Cambridge Crystallographic Data Centre.[18] We used a crystallographic information file (CIF) as input for the Crystal Explorer 17.5 software.[19] This software was utilized to calculate Hirshfeld surfaces and generate fingerprint plots. The standard surface resolution, along with parameters, such as dnorm, de, shape index, and curvedness, were noted. The 2D fingerprint plots were created based on the de and di distance scales displayed on the graph axes.

The ORTEP and packing diagrams of the β-chitin were generated using the Mercury software.[20] For all quantum calculations, Gaussian 09W[21] and GausView 5.0 software[22] were employed. Optimized geometry and electronic properties of β-chitin (as trimer) were made using the DFT method with B3LYP/6-31G (d,p), LC-BYLP/6-31G (d,p) and M06-2X/6-31G(d,p) basis sets based on the crystal structure. The analysis of non- and covalent interactions involved performing reduced density gradient (RDG) calculations and using interaction region indicators (IRI). This was conducted using Multiwfn software version 3.8.[23] The results were visualized with the assistance of visual molecular dynamics (VMD) software version 1.9.3.[24]

RESULTS AND DISCUSSION

Structure analysis

The crystal structure results of the β-chitin show that it has a monoclinic crystal system and $P112_1$ space group with intercepts of 4.8190(10) Å, 9.239 (2) Å and 10.384(2) Å, and has angles 90.00°, 90.00° and 97.16(5)°.[25] The three-unit model of β-chitin constructed in GaussView was optimized using DFT methods at the B3LYP/6-31G(d,p), LC-BLYP/6-31G(d,p), and M06-2X/6-31G(d,p) levels of theory, and the structure optimized with B3LYP/6-31G(d,p) is shown in Figure 1(a). The bond parameters of the optimized molecular structures were compared with those of the crystal structure and are presented in Table 1. Besides, both the computationally optimized geometry (as trimer) and the ORTEP diagram of the crystal structure for the β-chitin are shown in Figure 1 (a,b), respectively.

In Table 1, the bond parameters calculated by the B3LYP/6-31G(d,p), LC-BLYP/6-31G(d,p), and M06-2X/6-31G(d,p) levels of theory are compared with the bond parameters obtained from the crystal structure. There are six C–C bonds, ten C–H bonds, one N–H bonds, two N–C bonds, six C–O bonds, two O–H bonds in this compound. The highest bond length is observed at C4–C5 with 1.52 Å in the crystal structure. This bond length was found to be 1.5328 (B3LYP), 1.5314 (LC-BLYP) and 1.5269 (M06-2X) Å (C10-C11) in the optimized molecular structure, but the longest bond in this structure is between C7 and C8 atoms with a value of 1.54 Å (B3LYP). The shortest bond length is observed for the hydrogens bound to oxygen and nitrogen atoms (O3–H3A, O6–H6(0.82Å) and N1–H1A (0.86Å) in the crystal structure, and (O2–H42 (0.9747 Å (B3LYP), 0.9908 Å (LC-BLYP), 0.9711 Å (M06-2X)), O4–H43(0.9705 Å (B3LYP), 0.9842 Å (LC-BLYP), 0.9688 Å (M06-2X)) and N6–H44 (1.0126 Å (B3LYP), 1.0213 Å (LC-BLYP), 1.0121 Å (M06-2X)) in the optimized molecular structure. The O-H bond is particularly noteworthy due to its high polarity and effectiveness, which stem from significant differences in electronegativity. As the length of an atomic bond decreases, its strength and stability increase because the electrons are closer to the nucleus, resulting in a stronger bond between the atoms.

The most significant measured bond angles are found at O5-C13-C14 (123.298º (B3LYP), 123.7353º (LC-BLYP), 123.3428º (M06-2X)), O5-C13-N6 (122.3218° (B3LYP), 121.748° (LC-BLYP), 122.0272º (M06-2X)) and C8-N6-C13 (120.5658º (B3LYP), 119.6705º (LC-BLYP), 119.7041º (M06-2X)), highlighting the enhanced stability of these configurations. To better compare the bond lengths and bond angles of the β-chitin crystal structure and the trimer model constructed in GaussView, histogram diagrams were generated and are presented in Figure 2. According to Figure 2, it has been observed that the bond lengths in the crystal structure of β-chitin are generally slightly shorter than those calculated for the trimer structure modeled in GaussView, while the bond angles are slightly wider.

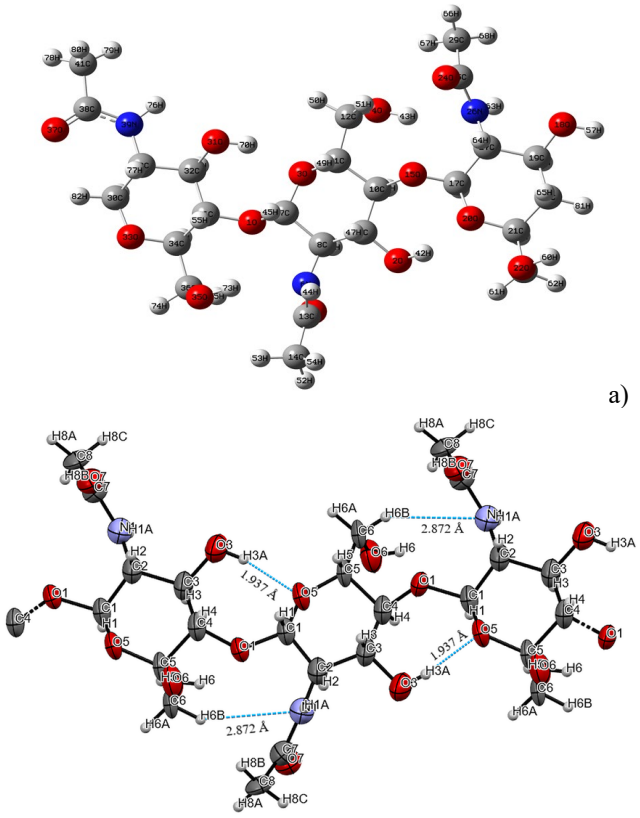

Figure 1: Optimized molecular geometry (a) and ORTEP diagram (b) of β-chitin (trimer)

Table 1
Experimental and theoretically calculated bond parameters for β-chitin

Bond lengths (Å)					
Crystal structure		Optimized molecular structure (as trimer)			
			B3LYP/6-31G (d,p)	LC-BYLP/6-31G (d,p)	M06-2X/6-31G(d,p)
Bond	Value	Bond	Value		
C1-H1	0.98	C7-H45	1.1048	1.1147	1.107
C1-C2	1.46(4)	C7-C8	1.5406	1.5393	1.5318
C1-O1	1.46(3)	O1-C7	1.3849	1.3863	1.3782
C1-O5	1.31(5)	O3-C7	1.4379	1.4518	1.4244
C2-H2	0.98	C8-H46	1.094	1.1045	1.0958
C2-C3	1.50(3)	C8-C9	1.5362	1.5317	1.5271
C2-N1	1.44(5)	N6-C8	1.4587	1.4603	1.4509
C3-H3	0.98	C9-H47	1.1068	1.1162	1.1065
C3-C4	1.50(4)	C9-C10	1.5333	1.5318	1.5254
C3-O3	1.40(3)	O2-C9	1.4108	1.4167	1.4036
C4-H4	0.98	C10-H48	1.0972	1.1068	1.0991
C4-C5	1.52(4)	C10-C11	1.5328	1.5314	1.5269
C4-O1	1.45(4)	C10-O15	1.4349	1.4417	1.4222
C5-H5	0.98	C11-H49	1.103	1.1115	1.1034
C5-C6	1.48(5)	C11-C12	1.5324	1.5313	1.5254
C5-O5	1.46(3)	O3-C11	1.4346	1.4436	1.423
C6-H6A	0.97	C12-H50	1.0947	1.1027	1.0944
C6-H6B	0.97	C12-H51	1.096	1.1048	1.0957
C6-O6	1.42(5)	O4-C12	1.4204	1.4293	1.4126
C7-C8	1.49(5)	C13-C14	1.5178	1.5153	1.5118
C7-N1	1.38(5)	N6-C13	1.3935	1.3986	1.3888
C7-O7	1.31(5)	O5-C13	1.2189	1.2295	1.2132

C8-H8A	0.96	C14-H53	1.0955	1.1039	1.0947
C8-H8B	0.96	C14-H52	1.0895	1.0961	1.0884
C8-H8C	0.96	C14-H54	1.0948	1.1013	1.0928
N1-H1A	0.86	N6-H44	1.0126	1.0213	1.0121
O1-C4	1.45(4)	O1-C16	1.4388	1.4458	1.4256
O3-H3A	0.82	O2-H42	0.9747	0.9908	0.9711
O6-H6	0.82	O4-H43	0.9705	0.9842	0.9688
Bond angles (º)					
Bond	Value	Bond		Value	
C2-C1-O1	110(3)	O1-C7-C8	108.5425	108.249	108.4345
C2-C1-O5	121(3)	O3-C7-C8	110.1164	110.0692	109.6296
O1-C1-O5	112(3)	O1-C7-O3	108.1513	108.4842	108.9682
C1-C2-C3	110(3)	C7-C8-C9	111.1359	110.6431	110.5012
C1-C2-N1	122(3)	N6-C8-C7	110.9636	110.5105	110.7623
C3-C2-N1	115(3)	N6-C8-C9	110.9262	110.9023	110.7212
C2-C3-C4	116(2)	C8-C9-C10	109.4848	108.6866	108.5972
C2-C3-O3	115(2)	O2-C9-C8	107.7426	107.9958	107.6899
C4-C3-O3	114(2)	O2-C9-C10	113.074	113.3114	113.2112
C3-C4-C5	113(3)	C9-C10-C11	109.9875	110.767	109.9738
C3-C4-O1	111(2)	C9-C10-O15	112.456	112.5182	112.9877
C5-C4-O1	103(2)	C11-C10-O15	107.042	106.5653	106.7864
C4-C5-C6	113(3)	C10-C11-C12	113.3172	112.3742	112.1245
C4-C5-O5	108(2)	O3-C11-C10	107.271	107.0209	107.555
C6-C5-O5	111(3)	O3-C11-C12	109.8593	110.0927	110.1216
C5-C6-O6	107(3)	O4-C12-C11	114.041	113.6485	113.2314
C8-C7-N1	118(3)	N6-C13-C14	114.2162	114.2506	114.4534
C8-C7-O7	125(3)	O5-C13-C14	123.298	123.7353	123.3428
N1-C7-O7	116(3)	O5-C13-N6	122.3218	121.748	122.0272
C2-N1-C7	128(3)	C8-N6-C13	120.5658	119.6705	119.7041
C1-O1-C4	119(2)	C7-O1-C16	118.3692	116.77	117.6808
C1-O5-C5	115(2)	C7-O3-C11	113.3124	111.5911	112.241
O1-C4-C3	111(2)	O1-C16-C32	112.2759	112.509	112.8593
O1-C4-C5	103(2)	O1-C16-C34	107.1022	106.5818	106.7324

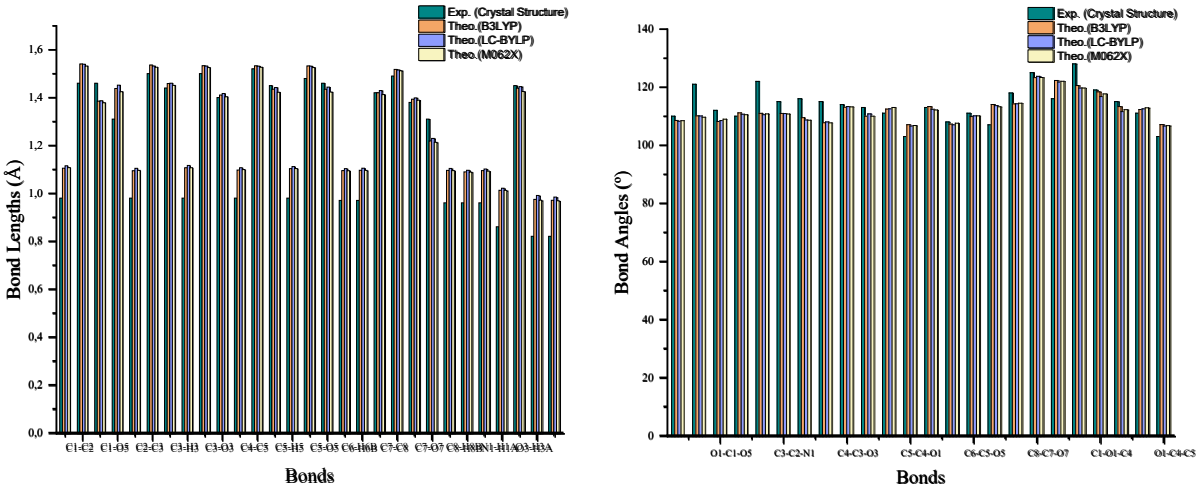

Figure 2: A comparison of experimental (from crystal structure) and theoretically calculated bond parameters for β-chitin

Crystal structure and packing of β-chitin

The Mercury software, a crystallography tool, was utilized to compute the geometric parameters and packing diagram. Figure 3 shows the packing diagram of β-chitin. The crystal structure of β-chitin exhibits a distinct non-planar geometry and manifests several non-covalent interactions with adjacent molecules within the crystalline packing. The existence of both intra- and intermolecular non-covalent interactions within the molecular

framework significantly enhances the overall stability of the crystal structure.

β-Chitin shows intramolecular interactions, involving O5···H3A-O3 and N1···H6B-C6 bonds.[25] In particular, the oxygen atom in the tetrahydropyran ring and the nitrogen atom in the secondary amide group form intramolecular hydrogen bonds with hydrogen atoms, with donor-acceptor distances of 1.937 Å and 2.872 Å, respectively, as noted in Figure 1 (b). Figure 3 shows the intermolecular hydrogen bonds, bond distances and crystal packing diagram of β-chitin. β-Chitin shows intermolecular interactions, involving C8-H8A···O3, O6-H6···O7, O7···H1A-N1, C8-H8C···O6, and O3-H3A···O5 bonds, with donor-acceptor distances of 2.515, 2.188, 2.047, 2.475 and 1.937 Å, respectively, as seen in Figure 3.

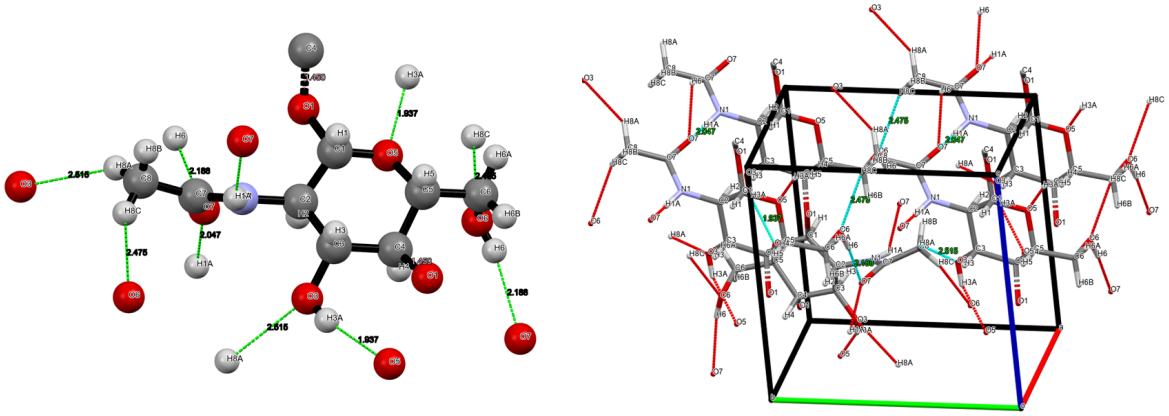

Figure 3: Crystal packing diagram of β-chitin with H-bond interactions

Hirshfeld surface analysis

In our current study, we used the Crystal Explorer 17.5 program to create Hirshfeld surfaces and the associated fingerprint plots. These surfaces were instrumental in determining the spatial occupation of a molecule within a crystal, enabling the partitioning of the crystal electron density into molecular fragments.[26] Furthermore, using Crystal Explorer (version 17.5) software, we conducted comprehensive 3D surface analysis and 2D molecular interaction studies of β-chitin. The resulting 3D maps illustrated normalized contact distance (dnorm), shape index, de, and curvedness for β-chitin, as depicted in Figure 4. Notably, the color-coded data represented various intermolecular contacts, with bright red spots highlighting hydrogen bond interactions and white areas indicating intermolecular distances close to van der Waals interactions (dnorm = 0).[27] The observed red-colored regions surrounding oxygen atoms and the hydrogen atom of the NH-C=O group indicate their involvement in hydrogen bonding interactions.

These findings were established through Hirshfeld surface analysis, which can be utilized to assess shape index and curvedness in both intra- and intermolecular interactions. In the context of the shape index, a qualitative measure of molecular shape, the atom situated in the concave red region assumes the acceptor position, while the atom located in the convex blue region takes on the donor position, defining the hydrogen bonding interactions.[28,29] Furthermore, the blue region on the curvedness surface is employed to estimate the surface shape. Visualization of the shape index and curvedness proves instrumental in ascertaining how molecules arrange themselves in relation to adjacent molecules.

The three-dimensional Hirshfeld surface showing the intermolecular interactions of β-chitin on the dnorm is shown in Figure 5. Additionally, the 2D fingerprint histogram illustrates the contact percentage of diverse molecular interactions, enabling a comprehensive analysis of the most significant interactions, including N···H, O···H, C···H, C···O, and H···H. This approach facilitates a comparison of the surface properties. Notably, Figure 6 provides a visual representation of the percentage of all interactions present in the molecule. According to Figure 6, H···H interactions is 48.8 percent, O···H/H···O is 44.8 percent, O···C/ C···O is 3.3 percent, C···H/H···C is 2.2 percent, N···H/ H···N is 0.8 percent in the fingerprint plot.

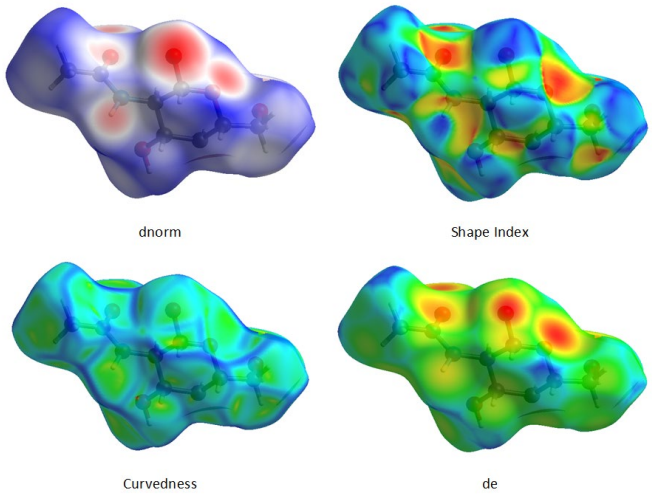

Figure 4: Hirshfeld surface mapped with d_{norm}, shape index, curvedness and d_e for β-chitin

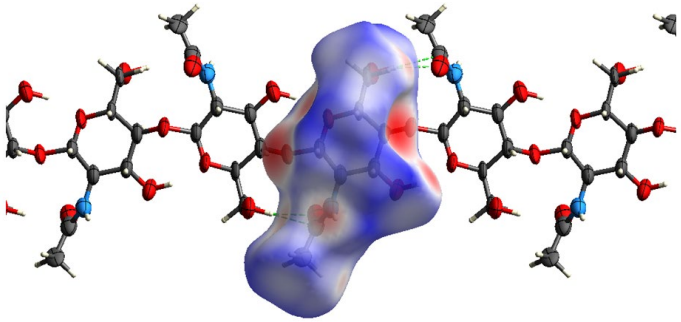

Figure 5: Three-dimensional Hirshfeld surface showing the intermolecular interactions of β-chitin on the d_{norm}

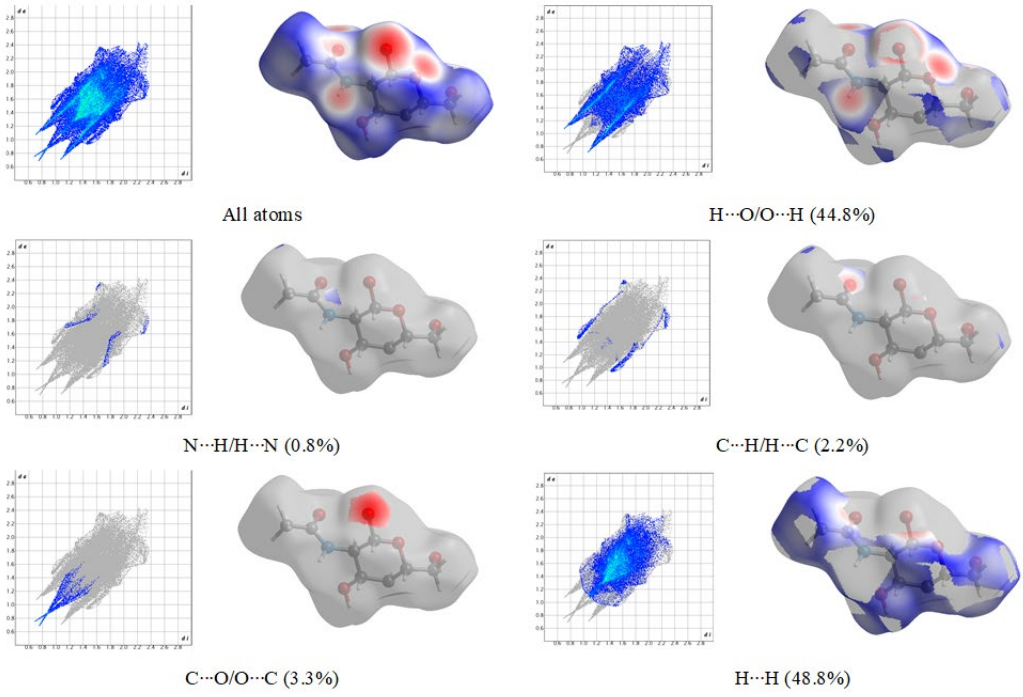

Figure 6: Fingerprint plots of β-chitin

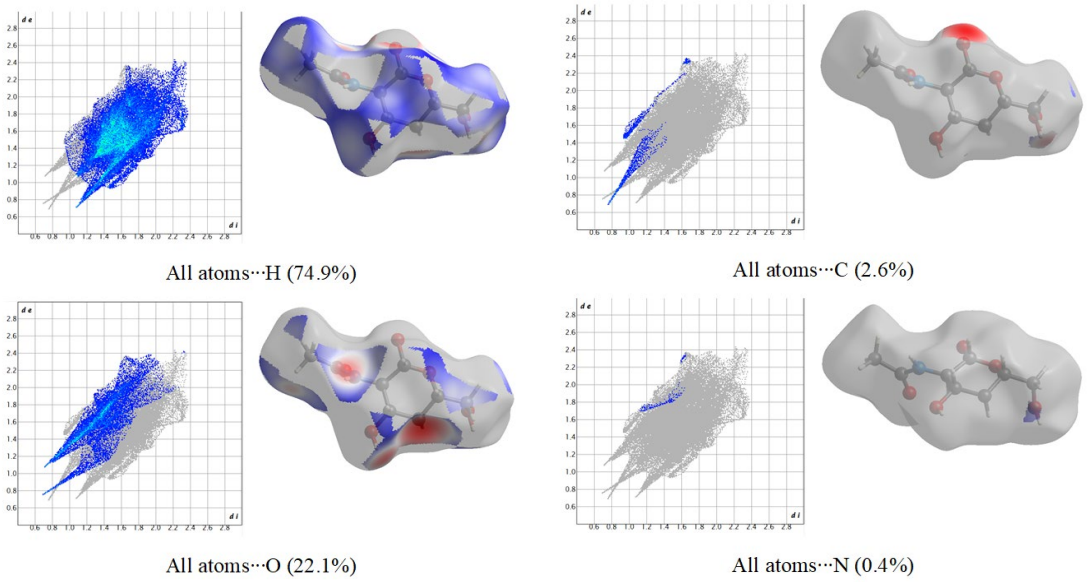

Figure 7: Fingerprint plots of β-chitin (each atom with all other atoms)

Figure 7 shows the percentage of interaction of each atom with all other atoms in the molecule. The contribution of all atoms···H interactions (74.9%), all atoms···O interactions (22.1%), all atoms···C interactions (2.6%), and all atoms···N interactions (0.4%) in the molecule. Based on the 2D fingerprint plot, it can be inferred that significant crystallization occurs as a result of H···H interactions, followed by O···H interactions.

RDG and IRI analyses

In order to gain a deeper understanding of both covalent and non-covalent interactions, we utilized Radiant Density Gradient (RDG) analysis and the interaction region indicator (IRI) for β-chitin. These methods have seen widespread use in current research.[30,31] NCI analysis proved to be a powerful tool for comprehending the non-covalent interactions within the molecule. The investigation of β-chitin involved the use of Multiwfn 3.8 programs, and the resulting isosurface plot was obtained from VMD software.

The RDG scattered graph was generated by plotting sign(λ^2)ρ against the reduced density gradient, where sign(λ^2)ρ represents the second eigenvalue of the electron density. Three regions were defined based on the values of sign(λ^2) and ρ. Strong interactions corresponded to halogen and hydrogen bonds with $\rho > 0$ and $\lambda < 0$, van der Waals interactions with $\rho \approx 0$ and $\lambda \approx 0$, and strong repulsion corresponded to steric effects with $\rho > 0$ and $\lambda > 0$. In essence, the nature of interactions was elucidated by the magnitude and symbol of sign(λ^2)ρ. Repulsive interactions were apparent when sign(λ^2)$\rho > 0$, attractive interactions were evident when sign(λ^2)$\rho < 0$, and van der Waals weak interactions were revealed when sign(λ^2)ρ equaled zero.[32,33] The scattered graph illustrated that the spikes around -0.02 and +0.01 a.u. represented the van der Waals force of attraction, while the spikes around 0.01 to 0.05 a.u. represented the steric effect within the ring. In addition, the spikes at the -0.025 to -0.05 atomic units range indicate a significant hydrogen bonding interaction within the molecule. Figure 8 provides evidence of steric effects and van der Waals interactions in β-chitin. The red spheres positioned at the center of the tetrahydropyran ring represent steric effects, while the blue spheres signify the strong O-H...O hydrogen bonding interaction present in the β-chitin molecule.

The presence of hydrogen bonds contributes to the increased stability of molecules. Analysis of the isosurface plot indicates the presence of weak non-covalent H•••H interactions, which are attributed to van der Waals forces. The IRI approach, facilitated by the Multiwfn 3.8 program, was utilized for this purpose. Different interaction regions can be identified by adjusting the isovalue for the IRI isosurfaces. This is possible because the IRI is based on the gradient norm of the electron density. In the RDG analysis, the sign(λ2)ρ function is used to visually represent the IRI isosurfaces using various colors, which help reveal different characteristic interaction regions. For example, Figure 8 (bottom) displays the color-coded interaction map of IRI versus sign(λ^2)ρ and the IRI isosurface map at IRI=1.1 isovalues for β-

chitin. The blue plate observed between O–H…O indicates a strong H-bonding interaction, with four spikes in the scatter map denoting the low-density, low-gradient region between −0.10 and −0.40 a.u. Also, the weaker N…O-H hydrogen bonding is represented as a bluish-green plate, and two spikes between 0 and 0.20 correspond to steric effects, while the spike around sign(λ2)ρ and ρ=0 is attributed to weak interatomic forces, such as van der Waals interactions. Finally, the IRI isosurfaces of carbon-carbon covalent bonds are visually depicted as blue cylindrical shapes in the isosurface image.

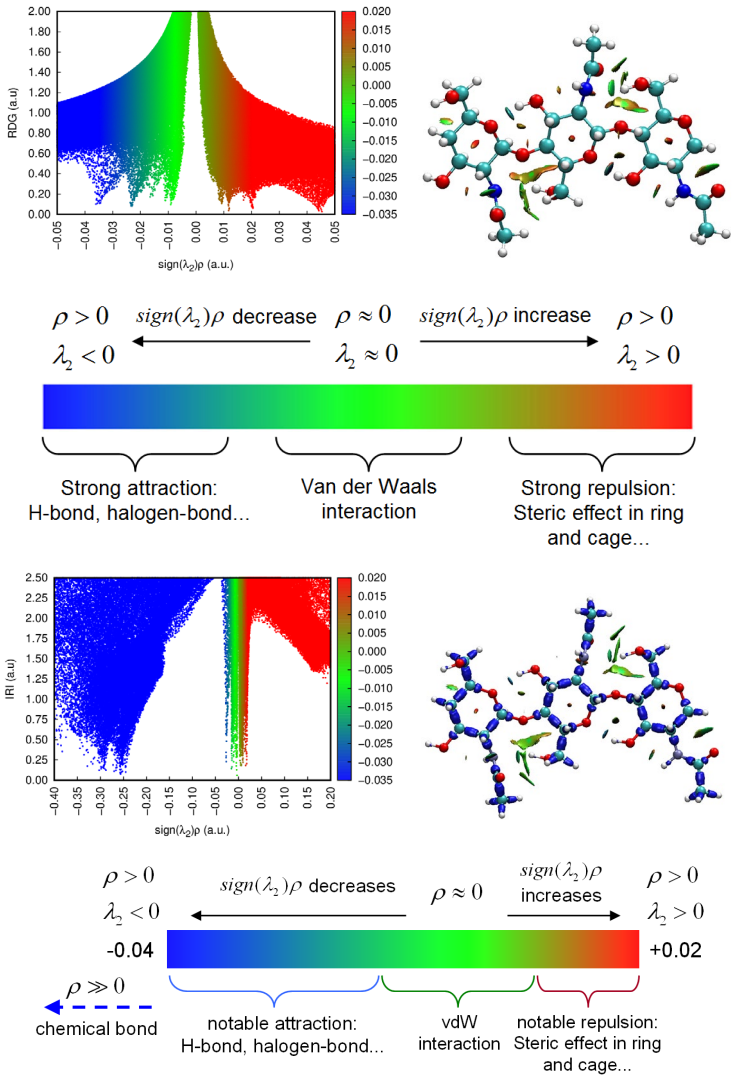

Figure 8: RDG (top) – IRI (bottom) analysis of β-chitin (trimer)

MEP and ALIE surface maps

The molecular electrostatic potential (MEP) map was generated using the DFT/M06-2X/6-31G(d,p) method to analyze the chemical reactivity and electron donor/acceptor sites of β-chitin, as well as to characterize its intermolecular interactions. MEP plots are widely utilized for predicting electrophilic and nucleophilic reaction regions, as well as hydrogen bonding interactions and biological recognition.[32-34] The MEP image illustrates (Fig. 9) that the most positive potential region in dark blue is located over hydrogens bound to nitrogen and oxygen, while the highest electronegative potential region in intense red is centered around carbonyl oxygen and oxygens. According to the MEP surface, carbonyl oxygen and oxygens with negative electrostatic potential act as hydrogen bond donors, while hydrogens with positive electrostatic potential serve as hydrogen bond acceptors. These reactive sites confirm the presence of intra- and intermolecular O···H-O, N···H-C, and N-H···O hydrogen bond interactions for β-chitin and highlight the significant role of these interactions in crystal

stabilization. In the case of β-chitin, oxygen atoms are implicated in electrophilic attacks, while the hydrogens attached to oxygen and nitrogen atoms are conducive to nucleophilic attacks.

Although MEP surfaces are commonly used to identify electrophilic attack-prone regions of molecules, ALIE surfaces are preferred for this purpose, as defined in the work by Politzer *et al.*[35,36] In general, ALIE provides information about the energy required to remove an electron from the molecule. Similar to the MEP descriptor, the ALIE is conveniently represented by mapping its values to the electron density surface, thus resulting in the ALIE surface. The average local ionization energy-mapped (ALIE-mapped) of β-chitin shown in Figure 10 indicates the most probable reaction sites that could interact with the electrically rich group, and the cyan spheres represent the minimum $\overline{I}$ surface.

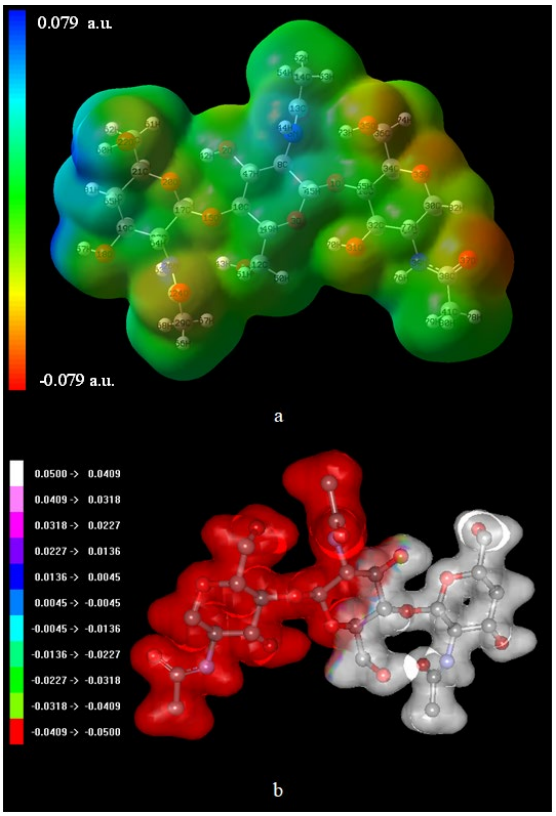

Figure 9: MEP maps of β-chitin (trimer) plotted with GaussView 5.0 (a) and ArgusLab (b)

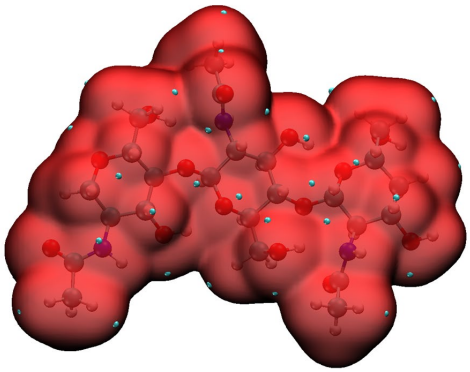

Figure 10: ALIE maps of β-chitin (trimer) plotted with Multiwfn

ELF and LOL analysis

The analysis of the electron localization function (ELF) and localized orbital locator (LOL) is crucial for understanding the atomic-shell structures, identifying chemical bonds, and validating charge-shifting bonds within

molecules.[32,37] Both ELF and LOL were comprehensively examined using the Multiwfn software.

In Figure 11, the ELF and LOL maps provide compelling evidence of electron presence in binding or non-binding interactions. The intense red color surrounding the hydrogen atoms in β-chitin indicates a concentration of bonding and non-bonding electrons, signifying significant electron placement due to covalent bonds, lone pairs, or the predominant nuclear shell in this region. The blue shading around carbon atoms denotes the cloud of displaced electrons, while the prominent blue circles visible around nitrogen and oxygen atoms indicate regions of electron depletion in the inner and valence layers. In the LOL plot, hydrogen atoms of β-chitin appear in white, signifying that the electron density surpasses the maximum allowable limit defined by the electron color chart. This observation emphasizes the substantial electron localization around these hydrogen atoms, offering valuable insight into the electron-rich nature of this region.

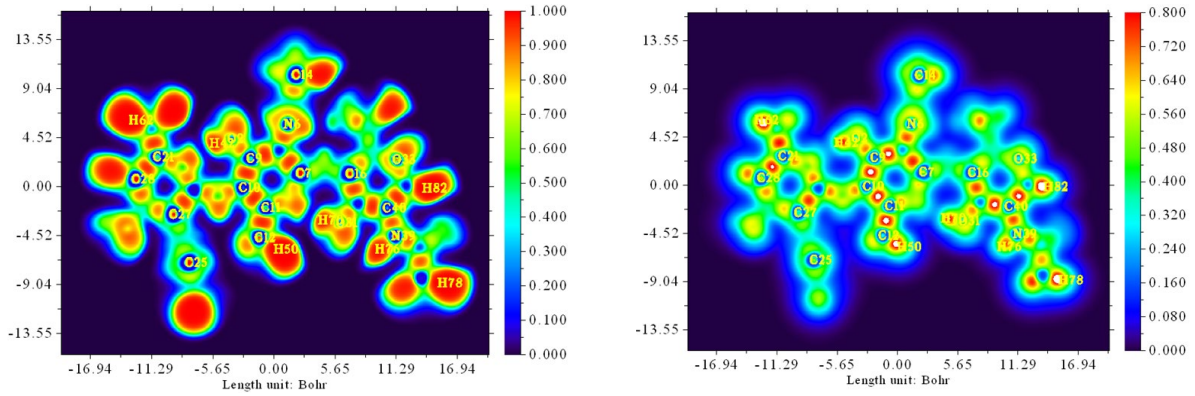

a) b)

Figure 11: ELF (a) and LOL (b) analyses of β-chitin (trimer)

HOMO-LUMO analysis

The HOMO and LUMO orbitals hold significant importance in quantum chemistry as they provide crucial insights into the interactions, kinetic stability, and chemical reactivity of molecules. The highest occupied molecular orbital (HOMO) and lowest unoccupied molecular orbital (LUMO) play indispensable roles in chemical reactions, serving as key parameters.[32,38] The theoretical calculation of HOMO and LUMO energies, along with other relevant parameters, was performed using the Density Functional Theory (DFT) method with B3LYP/6-31G (d,p), LC-BYLP/6-31G (d,p), and M06-2X/6-31G(d,p) basis sets. The obtained values for the β-chitin (as trimer) are detailed in Table 2. The 3D drawing of HOMO and LUMO molecular orbitals calculated by the M06-2X/6-31G(d,p) method for β-chitin is shown in Figure 12.

The LUMO is mainly localised on the acetamide group of a unit of β-chitin and the HOMO is mainly localised on the rest of the molecule, except for the CH_3 groups. The calculated energies of HOMO and LUMO for B3LYP/6-31G (d,p), LC-BYLP/6-31G (d,p) and M06-2X/6-31G(d,p) are -6.32 and 0.08, -8.10 and 1.31, -6.30 and 0.78 eV, respectively, and the energy gap of the β-chitin is found to be 6.40, 9.41 and 7.08 eV, respectively. In studies conducted in the literature, this value was found to be 7.41 eV,[39] and 8.125 eV[40] respectively.

The small energy gap of FMOs plays a role in the optical polarizability, chemical reactivity, softness and chemical hardness of the molecules.[41,42] When the results are compared, the smallest energy gap is obtained with the B3LYP method. The largest energy gap value was obtained with the M06-2X method. It is already given in the literature that the M06-2X method is more suitable for non-covalent interaction studies. Other electronic parameters, such as electronegativity, optical softness, chemical potential, ionization potential, electron affinity, hardness, softness, electrophilicity index, maximum charge transfer index[43-45] (as mentioned in our previous studies) were also calculated, and the data are presented in Table 2.

The electrophilicity index (ω) is a measure of a molecule's electrophilic power. It categorizes molecules as strong (ω>1.5 eV), marginal (ω<0.8 eV), or moderate (0.9 eV < ω < 1.4 eV).[42] The electrophilic index values calculated by B3LYP/6-

31G (d,p), LC-BYLP/6-31G (d,p) and M06-2X/6-31G(d,p) methods are 1.52, 1.07 and 1.22, respectively. In our literature surveys, this value was found to be 1.14 eV,[39] which is consistent with our results.

If we take the average of all three methods, we can say that the β-chitin (as trimer) can be a medium electrophile and can reveal biological activity.

Table 2
Some calculated electronic parameters of β-chitin using DFT with B3LYP/LC-BYLP/M062X-6-31(d,p) basis set

Parameters	Values (eV)		
	B3LYP	LC-BYLP	M062X
E_{HOMO}	-6.3207	-6.2962	-8.0976
E_{LUMO}	0.0781	0.7829	1.3113
Energy band gap (ΔE)	6.3988	7.0790	9.4089
Ionization energy (IP)	6.3207	6.2962	8.0976
Electron affinity (EA)	-0.0781	-0.7829	-1.3113
Electronegativity(χ)	3.1213	2.7567	3.3931
Chemical potential (μ)	-3.1213	-2.7567	-3.3931
Chemical hardness (η)	3.1994	3.5395	4.7044
Softness (ς)	0.3126	0.2825	0.2126
Electrophilicity index (ω)	1.5225	1.0735	1.2237
Maximum charge transfer index (ΔNmax)	0.9756	0.7788	0.7213
Optical softness ($\sigma_\circ$)	0.1563	0.1413	0.1063
Nucleophilic index (N)	0.6568	0.9316	0.8172

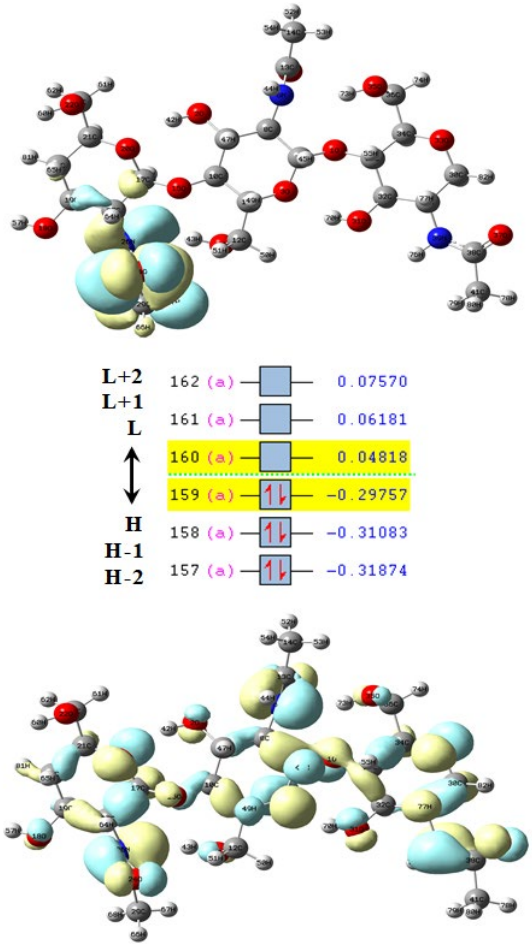

Figure 12: HOMO-LUMO energy diagram determined using M06-2X method of β-chitin (trimer)

CONCLUSION

Theoretical studies, such as molecular optimization, HOMO-LUMO, MEP, ALIE, Hirshfeld surface analysis and ELF, LOL, RDG and IRI analyses were conducted on β-chitin. The investigation showed that significant crystallization in β-chitin occurs due to H···H (48.8%) interactions, followed by O···H (44.8%) interactions. The optimized bond parameters calculated with the B3LYP/6-31G (d, p) method were compared with the bond parameters obtained from the crystal structure and it was seen that the results were quite close to each other.

Three calculation methods: B3LYP/6-31G (d,p), LC-BYLP/6-31G (d,p) and M06-2X/6-31G(d,p) were compared in terms of electronic properties. The lower energy value for the energy gap of β-chitin was found by the B3LYP/6-31G (d,p) method. MEP were carried out to identify the reactive regions of the β-chitin with a predominant H···H and O···H contribution in the crystal packing. RDG and IRI confirmed the existence of intramolecular O···H-O and N···H-O hydrogen bond interactions. In general, the theoretical analysis for the non-covalent interactions responsible for crystal packing provides a better understanding of molecular crystal packing. We think that the results of this study will help researchers to design and synthesize new materials, and the research can be extended to other commonly used biomaterials.

ACKNOWLEDGEMENTS: The author expresses gratitude to Bitlis Eren University for providing access to the Gaussian software.

REFERENCES

[1] A. Ibram, *Eur. J. Nat. Sci. Med.*, **4**, 97 (2021), https://doi.org/10.26417/805xka61j
[2] G. Satchanska, S. Davidova and P. D. Petrov, *Polymers*, **16**, 1159 (2024), https://doi.org/10.3390/polym16081159.
[3] A. Khan and K. A. Alamry, *Carbohyd. Res.*, **506**, 108368 (2021), https://doi.org/10.1016/j.carres.2021.108368
[4] M. S. Riaz Rajoka, L. Zhao and H. M. Mehwish, *Appl. Microbiol. Biotechnol.*, **103**, 1557 (2019), https://doi.org/10.1007/s00253-018-9550-z
[5] M. Kostag and O. A. El Seoud, *Carbohyd. Polym. Technol. Appl.*, **2**, 100079 (2021), https://doi.org/10.1016/j.carpta.2021.100079
[6] B. T. Iber, N. A. Kasan, D. Torsabo and J. W. Omuwa, *J. Renew. Mater.*, **10**, 1097 (2021), https://doi.org/10.32604/jrm.2022.018142
[7] H. Q. Peng, W. Zhu, W. J. Guo, Q. Li, S. Ma *et al.*, *Prog. Polym. Sci.*, **137**, 101635 (2023), https://doi.org/10.1016/j.progpolymsci.2022.101635
[8] P. Peluso and B. Chankvetadze, *Chem. Rev.*, **122**, 13235 (2022), https://doi.org/10.1021/acs.chemrev.1c00846
[9] T. T. C. Truong, B. Le, N. T. T. Duong, A. P. Le Thi and K. D. Nguyen, *Cellulose Chem. Technol.*, **58**, 283 (2024), https://doi.org/10.35812/cellulosechemtechnol.2024.58.27
[10] S. Zhang, F. X. Li and J. Y. Yu, *Cellulose Chem. Technol.*, **43**, 393 (2009), https://cellulosechemtechnol.ro/pdf/CCT9-10-2009/393-398.pdf
[11] M. K. Jang, B. G. Kong, Y. I. Jeong, C. H. Lee and J. W. Nah, *J. Polym. Sci. A – Polym. Chem.*, **42**, 3423 (2004), https://doi.org/10.1002/pola.20176
[12] M. Mincea, A. Negrulescu and V. Ostafe, *Rev. Adv. Mater. Sci.*, **30**, 225 (2012)
[13] S. I. Ahmad, R. Ahmad, M. S. Khan, R. Kant, S. Shahid *et al.*, *Int. J. Biol. Macromol.*, **164**, 526 (2020), https://doi.org/10.1016/j.ijbiomac.2020.07.098
[14] Y. W. Cho, J. Jang, C. R. Park and S. W. Ko, *Biomacromolecules*, **1**, 609 (2000), https://doi.org/10.1021/bm000036j
[15] Y. W. Cho, Y. N. Cho, S. H. Chung, G. Yoo and S. W. Ko, *Biomaterials*, **20**, 2139 (1999), https://doi.org/10.1016/S0142-9612(99)00116-7
[16] X. Hu, Y. Du, Y. Tang, Q. Wang, T. Feng *et al.*, *Carbohyd. Polym.*, **70**, 451 (2007), https://doi.org/10.1016/j.carbpol.2007.05.002
[17] Y. Zhao and D. G. Truhlar, *Theor. Chem. Acc.*, **120**, 215 (2008), https://doi.org/10.1007/s00214-007-0310-x
[18] https://www.ccdc.cam.ac.uk
[19] M. J. Turner, J. J. McKinnon, S. K. Wolff, D. J. Grimwood, P. R. Spackman *et al.*, CrystalExplorer17 (2017), University of Western Australia
[20] C. F. Macrae, I. Sovago, S. J. Cottrell, P. T. Galek, P. McCabe *et al.*, *Appl. Crystallogr.*, **53**, 226 (2020), https://doi.org/10.1107/S1600576719014092
[21] M. J. Frisch, G. W. Trucks and H. B. Schlegel, G. E. Scuseria, M. A. Robb *et al.*, Gaussian, Inc., Wallingford, CT (2010)
[22] R. Dennington, T. Keith and J. Millam, *GaussView*, Version 5, Semichem Inc., Shawnee Mission, KS (2010)
[23] T. Lu and F. Chen, *J. Comput. Chem.*, **33**, 580 (2012), https://doi.org/10.1002/jcc.22885
[24] W. Humphrey, A. Dalke and K. Schulten, *J. Mol. Graphics*, **14**, 33 (1996), https://doi.org/10.1016/0263-7855(96)00018-5
[25] D. Sawada, Y. Nishiyama, P. Langan, V. T. Forsyth, S. Kimura *et al.*, *Biomacromolecules*, **13**, 288 (2012), https://dx.doi.org/10.1021/bm201512t
[26] M. A. Spackman and D. Jayatilaka, *CrystEngComm*, **11**, 19 (2009), https://doi.org/10.1039/B818330A
[27] P. R. Spackman, M. J. Turner, J. J. McKinnon, S. K. Wolff, D. J. Grimwood *et al.*, *J. Appl. Crystallogr.*, **54**,

1006 (2021), https://doi.org/10.1107/S1600576721002910
[28] J. J. Koenderink and A. J. van Doorn, *Image Vis. Comput.*, **10**, 557 (1992), https://doi.org/10.1016/0262-8856(92)90076-F
[29] M. A. Spackman and J. J. McKinnon, *CrystEngComm*, **4**, 378 (2002), https://doi.org/10.1039/B203191B
[30] K. Palanisamy, S. Sundararaju, J. Sampathkumar and R. Rajamanickam, *J. Mol. Struct.*, **1306**, 137827 (2024), https://doi.org/10.1016/j.molstruc.2024.137827
[31] S. Celik and E. Tanıs, *Comput. Theor. Chem.*, **1212**, 113709 (2022), https://doi.org/10.1016/j.comptc.2022.113709
[32] F. Akman, *J. Mol. Model.*, **29**, 276 (2023), https://doi.org/10.1007/s00894-023-05684-4
[33] F. Akman, N. Issaoui and A. S. Kazachenko, *J. Mol. Model.*, **26**, 161 (2020), https://doi.org/10.1007/s00894-020-04423-3
[34] E. Scrocco and J. Tomasi, *Curr. Chem.*, **42**, 95 (1973), https://doi.org/10.1007/3-540-06399-4_6
[35] Y. Pang, X. Zhu, N. Li, H. Wang, Y. Li *et al.*, *Renew. Energ.*, **200**, 334 (2022), https://doi.org/10.1016/j.renene.2022.09.078
[36] P. Politzer, J. S. Murray and F. A. Bulat, *J. Mol. Model.*, **16**, 1731 (2010), https://doi.org/10.1007/s00894-010-0709-5
[37] T. Guan, C. Ren, Y. Feng, Y. Gao, N. Li *et al.*, *Food Bioprocess. Technol.*, **18**, 3329 (2025), https://doi.org/10.1007/s11947-024-03653-0
[38] I. Fleming, "Frontier Orbital and Organic Chemical Reactions", John Wiley and Sons, New York, 1976
[39] B. Messaoudi and S. Benykhlef, *Int. J. Chem. Technol.*, **8**, 164 (2024), https://doi.org/10.32571/ijct.1491250
[40] A. I. Barzic and R. M. Albu, *Polym. Bull.*, **78**, 6535 (2021), https://doi.org/10.1007/s00289-020-03406-x
[41] S. Abid, M. Khalid, M. Sagir, M. Imran, A. A. Braga *et al.*, *RSC Adv.*, **13**, 28076 (2023), https://doi.org/10.1039/d3ra04858f
[42] M. Khalid, S. Murtaza, K. Gull, S. Abid, M. Imran *et al.*, *RSC Adv.*, **14**, 1169 (2024), https://doi.org/10.1039/d3ra06673h
[43] F. Akman, *Cellulose Chem. Technol.*, **51**, 253 (2017), https://www.cellulosechemtechnol.ro/pdf/CCT3-4(2017)/p.253-262.pdf
[44] F. Akman, *Cellulose Chem. Technol.*, **53**, 243 (2019), https://doi.org/10.35812/CelluloseChemTechnol.2019.53.24
[45] F. Akman, A. Kazachenko and Y. Malyar, *Cellulose Chem. Technol.*, **55**, 41 (2021), https://doi.org/10.35812/CelluloseChemTechnol.2021.55.05